A numerical method for steady and nonisothermal viscoelastic fluid flow for high Deborah and Péclet numbers

Peter Wapperom
Martien A. Hulsen (corresponding author)
Jaap P.P.M. van der Zanden

Delft University of Technology
Faculty of Mechanical Engineering and Marine Technology
Laboratory for Aero and Hydrodynamics
Rotterdamseweg 145
2628 AL Delft (The Netherlands)

Abstract

A combined finite element / streamline integration method is presented for nonisothermal flows of viscoelastic fluids. The attention is focused on some characteristic problems that arise for numerical simulation of flows with high Deborah and Péclet numbers. The two most important problems to handle are the choice of an outflow boundary condition for not completely developed flow and the treatment of the dissipative term in the temperature equation. The ability of the numerical method to handle high Deborah and Péclet numbers will be demonstrated on a contraction flow of an LDPE melt with isotropic and anisotropic heat conductivity. The influence of anisotropic heat conduction and the difference between the stress work and mechanical dissipation will be discussed for contraction flows.

Keywords: nonisothermal viscoelastic flow; differential stress models; combined finite element / streamline integration; outflow boundary conditions; dissipation; anisotropic heat conduction

Introduction

Almost all modern industrial processes include nonisothermal flow of polymeric materials. Although the material functions of polymers highly depend on temperature, the attention in the area of numerical simulation has mainly been focused on isothermal flows. And when nonisothermal effects are taken into account, often a simplified temperature equation is assumed. For example, it is often assumed that the heat conduction is isotropic and that the internal heat production equals the stress work. This may be a good approximation for flows with low Deborah numbers, but for high Deborah numbers the anisotropic heat conduction due to orientation of the polymer chains, see for example van den Brule (1995), and the storage of mechanical energy may play a role. Because in polymer processing one often deals with high Deborah number flows it is interesting to be able to predict these nonisothermal effects.

Recently, Hulsen and van der Zanden (1991) developed a numerical code for steady, isothermal flow of viscoelastic fluids that is able to handle high Deborah numbers. For an LDPE melt, they could reach a Deborah number of 150. For nonisothermal flows at high Deborah numbers, in combination with high Péclet numbers, some characteristic problems arise. The aim of this paper is to describe the extension of the code of Hulsen and van der Zanden (1991) for nonisothermal flows, to discuss the problems that arise at high Deborah and Péclet numbers, and to show how to handle these numerically.

First we will describe the governing equations for nonisothermal viscoelastic fluid flow. Next we will discuss the numerical method that we use to solve these equations. Then we will apply the numerical method to a contraction flow of an LDPE melt and we will discuss the influence of the various terms in the temperature equation.

Governing equations

For the equations of motion and the stress constitutive equation we use well-known equations, see for example Bird *et al.* (1987). We shall restrict ourselves to the steady flow. The balance of mass then equals:

$$\nabla \cdot (\rho \boldsymbol{v}) = 0, \tag{1}$$

where ρ is the density and $\boldsymbol{v}$ the fluid velocity.

The balance of linear momentum equals

$$\rho \boldsymbol{v} \cdot \nabla \boldsymbol{v} + \nabla p = \nabla \cdot \boldsymbol{\tau}, \tag{2}$$

where p is the thermodynamic pressure and $\boldsymbol{\tau}$ the extra-stress tensor, which vanishes in equilibrium. The extra-stress tensor has to be specified by a constitutive equation. We will assume that it consists of a solvent part and a polymer part

$$\boldsymbol{\tau} = 2\eta_s \boldsymbol{d} + \boldsymbol{\tau}_{\mathrm{p}}, \tag{3}$$

with η_s the Newtonian solvent viscosity that may depend on temperature, $\boldsymbol{d} = (\boldsymbol{L} + \boldsymbol{L}^T)/2$ the Euler rate-of-deformation tensor with $\boldsymbol{L}^T$ the velocity gradient, and $\boldsymbol{\tau}_{\mathrm{p}}$ the polymer stress.

For the polymer stress we will assume a differential model of the type

$$\boldsymbol{\tau}_{\mathrm{p}} = G\left(\boldsymbol{b} - \boldsymbol{I}\right), \tag{4}$$

$$\boldsymbol{v} \cdot \nabla \boldsymbol{b} - \boldsymbol{L} \cdot \boldsymbol{b} - \boldsymbol{b} \cdot \boldsymbol{L}^T = -\frac{1}{\lambda}\boldsymbol{g}(\boldsymbol{b}), \tag{5}$$

where G is the shear modulus, $\boldsymbol{b}$ the configuration tensor, $\boldsymbol{I}$ the unit tensor, λ the relaxation time of the fluid, and $\boldsymbol{g}$ a nonlinear isotropic tensor function of the configuration tensor. Although not all differential models are covered by this equation, we will restrict ourselves to it because more extensive equations do not give rise to extra difficulties in the numerics of nonisothermal flow. For the Giesekus model, which we will use for our computations, the isotropic tensor function equals $\boldsymbol{g}(\boldsymbol{b}) = (\boldsymbol{I} + \alpha(\boldsymbol{b} - \boldsymbol{I})) \cdot (\boldsymbol{b} - \boldsymbol{I})$. For reasons of simplicity the polymer stress is assumed to consist of only one mode. However, the stress may consist of multiple modes, i.e. the polymer stress equals $\boldsymbol{\tau}_{\mathrm{p}} = \sum_{k=1}^{K} \boldsymbol{\tau}_k$, where each model stress is described by (4) and (5) with the index k the mode number. The relaxation time of the fluid depends exponentially on the temperature, and can be described by $\lambda = \lambda_{\mathrm{ref}} a_T$, with λ_{ref} the relaxation time at some reference temperature and a_T the Arrhenius or WLF shift factor, see for example Ferry (1981). The shear modulus G depends weakly on the temperature. We will assume that G is proportional to ρT^γ, with T the absolute temperature. The temperature scaling is well-known in rubber elasticity, see for example Treloar (1975). Due to the strong temperature dependence of the viscosity and relaxation time on temperature, the scaling can usually be neglected for the stress in (4). However, in the temperature equation this scaling may be important. Furthermore, for the scaling $G \simeq \rho T^\gamma$ the thermodynamic pressure only depends on density and temperature, see Wapperom and Hulsen (1997). So it is independent of the configuration tensor $\boldsymbol{b}$ and thus also of the polymer stress $\boldsymbol{\tau}_{\mathrm{p}}$.

The temperature equation for viscoelastic fluids has been derived from the thermodynamics in Wapperom (1996) and Wapperom and Hulsen (1997):

$$\rho c_{p,b}\, \boldsymbol{v} \cdot \nabla T = Q + T\beta \boldsymbol{v} \cdot \nabla p - \nabla \cdot \boldsymbol{\phi}_q, \tag{6}$$

2

where $c_{p,b}$ is the heat capacity at constant pressure and constant configuration tensor $\boldsymbol{b}$ and β the thermal expansion coefficient. It can be shown that $c_{p,b}$ approximately equals its equilibrium value, i.e. for $\boldsymbol{b} = \boldsymbol{I}$ for which it is usually denoted by c_p, see Wapperom and Hulsen (1997).

The internal heat production term Q consists of a positive irreversible part, the mechanical dissipation D_{m}, and a reversible part, a contribution caused by changes in the entropy due to orientation of the polymer chains. For the stress model (4), (5) the internal heat production term Q equals

$$Q = \gamma \boldsymbol{\tau} : \boldsymbol{d} + (1 - \gamma) D_{\mathrm{m}}, \tag{7}$$

$$D_{\mathrm{m}} = 2\eta_s \boldsymbol{d} : \boldsymbol{d} + \frac{1}{2\lambda} \left(\boldsymbol{\tau}_{\mathrm{p}} \cdot \boldsymbol{b}^{-1} \right) : \boldsymbol{g}, \tag{8}$$

where γ is the exponent of the temperature dependence of $G \simeq \rho T^\gamma$, as discussed above. For $\gamma = 0$ the internal heat production term Q reduces to the dissipation D_{m} and the fluid is called energy elastic. For $\gamma = 1$, Q reduces to the stress work $\boldsymbol{\tau} : \boldsymbol{d}$ and the fluid is called entropy elastic. See also Braun (1991). We will only consider these two cases. Other values of γ are just a linear combination of these terms and therefore do not cause extra difficulties. The difference between the stress work and the mechanical dissipation is usually large in developing flows at high Deborah numbers, i.e. $\boldsymbol{v} \cdot \nabla \boldsymbol{b}$ is large in Eq. (5). A more detailed discussion and the expressions for D_{m} for various stress models can be found in Wapperom (1996) or Wapperom and Hulsen (1997).

The pressure term is usually not taken into account for viscoelastic fluids. It represents the effect that the temperature of every (compressible) material increases during compression and decreases during expansion. Due to the high viscosity of polymeric fluids it is usually not small, not even in shear flows. Then $\boldsymbol{v} \cdot \nabla p$ is, just as the stress work, proportional to $\eta V^2 / L$ with η, V and L a characteristic viscosity, velocity and length. Typical values for $T\beta$ of viscoelastic fluids are in the range $0.1 < T\beta < 0.25$, see van Krevelen and Hoftyzer (1976), so that the order of magnitude is about 10 to 25% of the stress work. So even in shear flows this term cannot be neglected a priori. Note that the trace of the polymer stress, does not contribute to the pressure term, but only to the heat production term Q.

For the heat flux $\boldsymbol{\phi}_q$ we will assume a Fourier type of constitutive equation:

$$\boldsymbol{\phi}_q = -\boldsymbol{\kappa}(\boldsymbol{b}, T) \cdot \nabla T, \tag{9}$$

where $\boldsymbol{\kappa}$ is the heat conduction tensor which may be anisotropic due to orientation of the polymer chains. In simple shear and elongation flows it is observed that the thermal conductivity increases in the direction of orientation and decreases in the direction perpendicular to the orientation, see for example Choy et $al.$ (1981) and Wallace et $al.$ (1985). The physical model behind the anisotropy is that energy can be transported more readily through the backbone of the polymer chains than from one chain to another. The anisotropy can be described by a dependence of the heat conduction tensor on $\boldsymbol{b}$ that is a measure for the orientation. We will assume a linear relation between the heat conduction tensor and the configuration tensor:

$$\boldsymbol{\kappa} = \kappa_{\mathrm{eq}} \boldsymbol{I} + \kappa_1 (\boldsymbol{b} - \boldsymbol{I}), \tag{10}$$

with κ_{eq} the equilibrium thermal conductivity that is usually tabulated and κ_1 a constant, see for example van den Brule (1995). For high Deborah numbers the configuration tensor $\boldsymbol{b}$ is far from unity, so that the heat conduction tensor may differ considerably from the equilibrium value, for not too small values of κ_1.

As noted above, we have $p = p(\rho, T)$ or equivalently $\rho = \rho(p, T)$, the balance of mass becomes

$$-\beta \left. \frac{\partial \rho}{\partial T} \right|_p \dot{T} + \kappa_T \left. \frac{\partial \rho}{\partial p} \right|_T \dot{p} = -\nabla \cdot \boldsymbol{v}, \tag{11}$$

3

where κ_T is the isothermal compressibility. For polymers the order of magnitude of the compressibility is small, 10^{-10} Pa $< \kappa_T < 10^{-9}$ Pa, so that the $\dot{p}$ term will be neglected in the balance of mass. The order of magnitude of the thermal expansion coefficient is 10^{-4} K$^{-1} < \beta < 10^{-3}$ K^{-1} for polymers. For large $\dot{T}$, or $\boldsymbol{v} \cdot \nabla T$ for steady flow, the thermal expansion term might be important. However, because of the high Péclet numbers for flows of polymeric fluids, $\boldsymbol{v} \cdot \nabla T$ is usually small and we will neglect this term henceforth. Then the balance of mass (11) reduces to the incompressibility condition

$$\nabla \cdot \boldsymbol{v} = 0, \tag{12}$$

and the only term concerning the temperature dependence of the density is the $T\beta \boldsymbol{v} \cdot \nabla p$ term in the temperature equation. Note that ∇p does not include any terms with invariants of the stress $\boldsymbol{\tau}$, because of $p = p(\rho, T)$.

The numerical method

In this section we will describe the numerical method that we use to solve the system of partial differential equations described in the previous section.

In order to use different solution methods for the elliptic part of the equations (a finite element method for the balance equations) and the hyperbolic part (a streamline integration method for the differential equation for the configuration tensor), we will decouple the system of equations. We will solve these decoupled equations with the help of an iterative method. An additional advantage over solving the whole system at once is that less memory is needed, because only two small system matrices are required (for velocity and temperature) instead of one big system matrix (for velocity, temperature and all the modal stresses). Particularly for multi-mode models, which are often needed to obtain a good description of the fluid behaviour, a decoupled method is needed to avoid excessive use of memory. On the other hand, however, for high Deborah numbers the rate of convergence may be low due to the splitting and the iterated solution is somewhat less accurate. Therefore a large number of relatively cheap iterations has to be performed to obtain a converged solution. Dependent on the problem the number of iterations is between 30 and 200.

The iterative scheme
The outline of the iteration process that we use to solve the decoupled equations is as follows:

1. Start with an initial field for the velocity, the configuration tensor and the temperature. This may be a result of a previous calculation. If there is no starting field of a previous simulation available, a zero velocity, a zero stress ($\boldsymbol{b} = \boldsymbol{I}$), and a reasonable initial guess for the temperature (for example the temperature of a Dirichlet boundary condition or the reference temperature) may be taken as the initial field.

2. Perform an iteration step. An iteration step $(i + 1)$ of the iteration process consists of the following four substeps, which are performed after each other

   - Calculate the updated velocity field, by solving a matrix-vector equation for the equations of motion (12) and (2): $A_v \Delta \mathcal{V}^{i+1} = -R_v(\mathcal{V}^i, \mathcal{T}^i, \Upsilon^i)$. The discretisation method and the implementation in the iterative scheme will be discussed briefly further on.
   - Calculate the updated temperature field, by solving a matrix-vector equation for the temperature equation (6): $A_T \Delta \mathcal{T}^{i+1} = -R_T(\mathcal{V}^{i+1}, \mathcal{P}^{i+1}, \mathcal{T}^i, \mathcal{B}^i)$. The discretisation method and the implementation in the iterative scheme will be discussed further on.
   - Calculate the updated configuration tensor field, by solving an equation of the form (5): $\mathcal{B}^{i+1} = f(\mathcal{V}^{i+1}, \mathcal{T}^{i+1}, \mathcal{B}^i)$ and calculate the polymer stress Υ^{i+1}. The discretisation method and the implementation in the iterative scheme will be discussed briefly further on.
   - Calculate an approximation of the normal stress σ_n at the outflow boundary. This step will be explained in more detail further on.

4

$\mathcal{V}$, $\mathcal{T}$, $\mathcal{B}$, Υ and $\mathcal{P}$ are vectors with the nodal point values of the discretised velocity, the temperature, the configuration tensor, the polymer stress and the pressure.

3. Repeat step 2 until the solution has converged.

Next we will briefly describe the solution methods for the equations of motion and the stress constitutive equation, because they are almost identical to the solution methods for isothermal flows. Then we will focus on the numerical method for the temperature equation and the outflow boundary conditions.

The equations of motion
The numerical method to solve the equations of motion and the stress constitutive equation is essentially the same as the method described by Hulsen and van der Zanden (1991) for isothermal viscoelastic flow. Therefore, we will only give a short overview of this part of the solution method. The full details are described in Hulsen and van der Zanden (1991).

To discretise the equation of motion, we use the standard Galerkin method with the Crouzeix–Raviart element ($P_2^+ - P_1$), i.e. seven velocity nodes and one pressure node with the pressure and two derivatives. The pressure derivatives and the velocities in the centre point can be eliminated on element level. The pressure in the centre point will be eliminated with the help of the penalty method. Instead of the divergence equation (12), a slightly perturbed equation $\epsilon_p p + \nabla \cdot \boldsymbol{v} = 0$ is solved. In discretised form it becomes

$$\epsilon_p D\mathcal{P} = L\mathcal{V}, \tag{13}$$

where the penalty parameter ϵ_p is a small parameter, D the pressure mass matrix and L the continuity matrix. For our calculations we have used $\epsilon_p \Delta p \simeq 10^{-6}$, where Δp is the maximum pressure difference in the flow. For an extensive description of the Crouzeix–Raviart element and the penalty method, refer to Cuvelier *et al.* (1986). After applying the Gauss divergence theorem to the Galerkin terms of both the divergence of the stress and gradient of the pressure and after elimination of the pressure, a matrix-vector equation of the following form is obtained:

$$N_v(\mathcal{V}) + (\eta_s(\mathcal{T})S_v + C_v)\,\mathcal{V} + Q(\Upsilon) = F_v, \tag{14}$$

where N_v is a nonlinear operator due to the convective acceleration, S_v a linear operator due to the viscous stress, $C_v = \epsilon_p^{-1} L^T D^{-1} L$ the penalty matrix, Q a function of the viscoelastic stress and F_v contains the contributions of the natural boundary conditions.

To solve the discretised equations of motion (14) we use an incremental formulation:

$$A_v^i \Delta \mathcal{V}^{i+1} = \left(M_v(\mathcal{V}^i) + \eta_{\text{it}}(\mathcal{T}^i)S_v + C_v\right) \Delta \mathcal{V}^{i+1} = -R_v(\mathcal{V}^i, \Upsilon^i, \mathcal{T}^i), \tag{15}$$

where the Picard iteration matrix A_v^i contains contributions of a linearization of the convective terms M_v with the velocity gradient on level $i+1$ and the velocity on level i, a viscous matrix $\eta_{\text{it}} S_v$ and the penalty matrix C_v. The iteration viscosity η_{it} is only a relaxation parameter that slows down the iteration process, but is necessary to obtain a convergent solution method. For isothermal calculations $\eta_{\text{it}} = \eta_0$ or $\eta_{\text{it}} = 2\eta_0$, where η_0 is the zero-shear-rate viscosity, is often a good choice. For nonisothermal calculations the spatial temperature distribution may be strongly non-homogeneous. This results in large differences of the viscosity in the flow. To take into account this temperature effect for the iteration viscosity, a similar temperature dependence of $\eta_{\text{it}} = \eta_{\text{it,ref}} a_T$ may be taken. For very simple flows of viscoelastic fluids and for Newtonian flows, this gave a considerable acceleration of convergence. However, for viscoelastic fluids in a 4:1 contraction no convergence could be obtained, unless $\eta_{\text{it,ref}}$ was increased considerably. No acceleration of convergence could be obtained in this way. The increment of the velocities is defined by $\Delta \mathcal{V}^{i+1} =$

$\mathcal{V}^{i+1} - \mathcal{V}^i$. The residual of the equations of motion $R_v(\mathcal{V}^i, \Upsilon^i, \mathcal{T}^i)$ depends on the discrete velocities $\mathcal{V}^i$, the stress Υ^i and the temperatures $\mathcal{T}^i$ of a former iteration step:

$$R_v(\mathcal{V}^i, \Upsilon^i, \mathcal{T}^i) = \left(N_v(\mathcal{V}^i) + \eta_s(\mathcal{T}^i) + \eta_{\mathrm{co}}(\mathcal{T}^i)\right) S_v \mathcal{V}^i + C_v \mathcal{V}^i + Q(\Upsilon^i - 2\eta_{\mathrm{co}}(\mathcal{T}^i)\bar{D}^i) - F_v. \quad (16)$$

From the vector Q with the contributions of the viscoelastic stress, an extra diffusive term, based on the nodal point averages of the rate-of-deformation tensor $\bar{D}^i$, has been subtracted. An analogous term based on the non-averaged velocity gradients has been added to the contribution of the solvent. The extra viscosity η_{co} is necessary to avoid almost zero effective viscosities, see Hulsen and van der Zanden (1991). For isothermal calculations $\eta_{\mathrm{co}} = \eta_0 - \eta_s$ is often a good choice. As for the iteration viscosity a temperature dependent η_{co} only gave an acceleration of convergence in simple flows.

For detecting convergence both the increment and the residual have to be small:

$$\frac{\max_j |\Delta \mathcal{V}_j^{i+1}|}{\max_j |\mathcal{V}_j^{i+1}|} \leq \epsilon_{v,\mathrm{inc}}, \qquad \frac{||R_v(\mathcal{V}^i, \Upsilon^i, \mathcal{T}^i)||_f}{||R_v(\mathcal{V}^i, \Upsilon^i, \mathcal{T}^i)||_t} \leq \epsilon_{v,\mathrm{res}},$$

where the maximum norm $|.|$ has been taken over all nodal points j. The norm $|| \cdot ||_f$ denotes the Euclidean norm over the free degrees of freedom, without the essential boundary conditions. The norm $|| \cdot ||_t$ denotes the Euclidean norm over the total degrees of freedom, including the essential boundary conditions. $\epsilon_{v,\mathrm{inc}}$ and $\epsilon_{v,\mathrm{res}}$ are small parameters. In all our calculations we take $\epsilon_{v,\mathrm{inc}} = \epsilon_{v,\mathrm{res}} = \mathcal{O}\left(10^{-3}\right)$.

The stress constitutive equation
A stress differential model can be written as an ordinary differential equation for the configuration tensor, by applying the method of characteristics. For a steady flow the characteristics are equal to the streamlines. Equation (5) can then be written as

$$\frac{d\boldsymbol{b}}{ds}\frac{ds}{dt} = \boldsymbol{G}(\boldsymbol{v}, \boldsymbol{L}^T, \boldsymbol{b}, T), \quad (17)$$

where s is a streamline parameter and $\boldsymbol{G}$ a tensor function that depends on the constitutive model. On the whole the nonisothermal streamline integration method is similar to the isothermal streamline integration method described by Hulsen and van der Zanden (1991). It only differs in the following aspects. Due to the (strong) temperature dependence of the time constant λ, the tensor function $\boldsymbol{G}$ in (17) is a function of temperature. Therefore the temperature along the streamline has to be known. These temperatures are obtained by quadratic interpolation of the nodal point values of the element in which the part of the streamline is. Then the stepsize depends on the temperature as well, because it is based on the stability region of the linearised form of (17). Furthermore, the maximum travel time (magnitude of the particle trajectory) and the maximum integration length have been limited by $3\lambda_{\mathrm{ref}}a_T$, evaluated at the end point of the streamline, instead of the $3\lambda_{\mathrm{ref}}$ for the isothermal calculations. This avoids too long and too short maximum travel times and integration lengths in case of large temperature differences in the flow. Finally, after solving the differential equation for the configuration tensor, the temperature is needed to calculate the polymer stress (4), because the modulus G may depend on temperature.

The temperature equation
One of the main aspects in the temperature equation is the dominance of the convective term for most flows, due to the high value of $\rho c_{p,b}/\kappa = \mathcal{O}(10^7)$ m$^{-2} \cdot$s, for flows of polymeric fluids. To handle the dominance of the convection, the streamline upwind Petrov–Galerkin (SUPG) method has been used, see for an extensive description Brooks and Hughes (1982) or Hughes and Brooks

(1982). For this method all terms are multiplied by a discontinuous test function in the direction of the flow $\psi_u = \tau \boldsymbol{v} \cdot \nabla \psi$, integrated over all element interiors and added to the Galerkin formulation. The upwind function τ determines the amount of upwind and ψ is the test function. Then an equation of the following form results:

$$\int_\Omega \left(\rho c_{p,b} \, \boldsymbol{v} \cdot \nabla T - Q \right) \psi + \left(\boldsymbol{\kappa} \cdot \nabla T + T \beta p \boldsymbol{v} \right) \cdot \nabla \psi d\Omega +$$

$$\sum_{e=1}^{N} \int_{\Omega_e} \left(\rho c_{p,b} \, \boldsymbol{v} \cdot \nabla T - \nabla \cdot \left(\boldsymbol{\kappa} \cdot \nabla T \right) - Q - T \beta \boldsymbol{v} \cdot \nabla p \right) \psi_u d\Omega_e =$$

$$\int_\Gamma \left(\boldsymbol{n} \cdot \boldsymbol{\kappa} \cdot \nabla T + T \beta p \boldsymbol{n} \cdot \boldsymbol{v} \right) \psi d\Gamma, \qquad \forall \psi \in \Psi, \quad \forall \psi_u \in \Psi_u, \quad (18)$$

where Ω is the integration area with boundary Γ, Ω_e the interior of an element and N the number of elements. The Gauss divergence theorem has been applied to the Galerkin terms of both the second derivative of the temperature and the pressure term. The integrands of the boundary integrals have to be prescribed along boundaries with natural boundary conditions.

Next we will focus on the numerical implementation of the terms that are usually not taken into account in numerical simulations of polymeric fluids: the anisotropy of the heat conduction tensor, the dissipative term, and the pressure term.

The heat conduction term
The heat flux has three contributions in (18), two from the Galerkin test functions and one from the SUPG test functions. To the latter term the Gauss divergence theorem can not be applied, because the upwind test function ψ_u depends on the gradient of the test function ψ, which is a piecewise polynomial, and is therefore discontinuous across the element boundaries. The implementation of the anisotropy is straightforward and does not give any serious problems.

Calculation of the mechanical dissipation
For $\gamma \neq 1$ the internal heat production term Q is not equal to the stress work, and the mechanical dissipation has to be calculated. This may lead to serious problems. For many stress models the expression for the mechanical dissipation, (8), contains a term with $\operatorname{tr} \boldsymbol{b}^{-1} = I_2/I_3$. Theoretically this term should not give any problems, because the configuration tensor is positive definite. However, due to numerical approximation errors the positive definiteness may be lost. Particularly if I_3 becomes close to zero this may lead to very large numerical errors or even arithmetic overflows. The causes and the ways to solve these problems will be discussed next.

A first cause of the indefiniteness of a configuration tensor is that due to the (quadratic) interpolation of a (positive definite) configuration tensor from the nodal points to the integration points the positive definiteness may be lost. Particularly, large gradients in an element may cause indefinite configuration tensors in the integration points. This occurs for example at the start-up from a zero-velocity initial field with fully developed boundary conditions at the inflow. These large errors can be avoided when the mechanical dissipation is first calculated in the nodal points and then interpolated to the integration points. However, this procedure reduces the accuracy of the calculation of the finite element integrals and will therefore be restricted to the integration points where $\boldsymbol{b}$ is indefinite.

A second cause is that during the streamline integration the configuration tensor in some nodal point has become indefinite due to numerical approximation errors. This occurs especially in regions where large gradients are present, for example near sharp corners. To avoid nonlinear instabilities in the streamline integration, the configuration tensor is then corrected with a 2D isotropic term to a semi-positive definite tensor, as described in Hulsen and van der Zanden (1991) and sketched in Fig. 1. However, a vanishing determinant is rather disastrous for the inverse of the configuration tensor and some other correction method should be applied. Therefore we use the
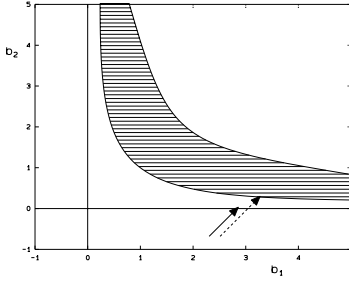
Figure 1: Correction of the configuration tensor in 2D. b_1 and b_2 are the principal values of $\boldsymbol{b}$. The solution of the model lies in the dashed area, which is bounded by two lines with constant I_3. The solid arrow is the projection on the first quadrant used by Hulsen and van der Zanden (1991). The dashed arrow is a projection on the lower bound I_3^{min}.

results of Wapperom and Hulsen (1995), who have shown that for most of the well-known stress models it is possible to find a positive lower bound for the determinant I_3^{min}. Then we correct the configuration tensor, with a 2D isotropic term, to a positive definite tensor with determinant $I_{3,\mathrm{min}}$. For most of the models the lower bound is $I_3^{\mathrm{min}} = 1$, which corresponds to the value in equilibrium. For the 2D Giesekus model, however, the lower bound depends on the parameter α of that model, see Hulsen (1988). For the 3D Giesekus model and the FENE-P model it is not possible to find such a lower bound and one has to proceed differently. For these models we then take the stress work instead of the mechanical dissipation of the viscoelastic model $D_{\mathrm{m}}^{\mathrm{p}}$, or if a multiple mode model is used we take the stress work of the mode instead of the dissipation of the mode.

A very small positive value of the determinant may also cause large numerical errors in the mechanical dissipation. Therefore the correction has to be performed for small positive determinants as well.

Calculation of the pressure

The pressure is piecewise linear per element. It is discontinuous over the element boundaries and therefore integrated by parts. In the equations of motion the pressure gradient in the centre point of an element has been eliminated with the help of the centre point velocities of that element. It can easily be recomputed on element level with the nodal point velocities, see Cuvelier *et al.* (1986). The pressure in the centre point has been eliminated on element level with the help of the penalty method. It can be recomputed with the inverse of the operation used to eliminate the pressure in the equations of motion (13). The pressures in the integration points of an element are then obtained from a linear interpolation of the pressure and its derivatives in the centre point of that element. The boundary integral with the pressure only contributes to the temperature equation at an inflow or outflow boundary, where natural boundary conditions are imposed. Only for viscoelastic models with a vanishing second normal stress difference the pressure is constant in fully developed shear flows. Otherwise the boundary integral has to be evaluated. We will discuss its implementation in more detail in the section about outflow boundary conditions.

Discretisation method

Substitution of the finite element approximation in the temperature equation (18) results in a matrix-vector equation of the form

$$N_T(\mathcal{V}, \mathcal{T}) + S_T(\mathcal{B}, \mathcal{T})\mathcal{T} = F_T(\mathcal{V}, \mathcal{T}, \mathcal{B}, \mathcal{P}), \tag{19}$$

with N_T a nonlinear operator due to the convective term and S_T an operator due to heat conduction. S_T may depend on the configuration tensor and linearly on the temperature, via the heat conduction

tensor. The right-hand-side vector F_T consists of contributions of the natural boundary conditions and the internal heat production Q.

To solve the discretised temperature equation (19) an incremental formulation has been used:

$$\left(\kappa_{\mathrm{it}} S_T^{\mathrm{it}} + S_T(\mathcal{B}^i, \mathcal{T}^i) + M_T(\mathcal{V}^{i+1}, \mathcal{T}^i)\right) \Delta \mathcal{T}^{i+1} = -R_T(\mathcal{V}^{i+1}, \mathcal{B}^i, \mathcal{T}^i, \mathcal{P}^{i+1}), \qquad (20)$$

where all of the matrices and the right-hand-side vector contain contributions of the upwind scheme. The Picard iteration matrix consists of the convective matrix M_T, the diffusive matrix S_T and an extra diffusive matrix $\kappa_{\mathrm{it}} S_T^{\mathrm{it}}$. The iteration diffusivity κ_{it} slows down the iteration process, but is sometimes necessary to obtain a convergent solution method. A constant and isotropic iteration diffusivity $\kappa_{\mathrm{it}} = \kappa_{\mathrm{eq}}$ is often sufficient. The increment of the temperature is defined by $\Delta \mathcal{T}^{i+1} = \mathcal{T}^{i+1} - \mathcal{T}^i$ and the residual $R_T(\mathcal{V}^{i+1}, \mathcal{B}^i, \mathcal{T}^i, \mathcal{P}^{i+1})$ of the temperature equation equals

$$R_T(\mathcal{V}^{i+1}, \mathcal{B}^i, \mathcal{T}^i, \mathcal{P}^{i+1}) = S_T(\mathcal{B}^i, \mathcal{T}^i)\mathcal{T}^i + N_T(\mathcal{V}^{i+1}, \mathcal{T}^i) - F_T(\mathcal{V}^{i+1}, \mathcal{B}^i, \mathcal{T}^i, \mathcal{P}^{i+1}). \qquad (21)$$

For detecting convergence both the increment and the residual have to be small:

$$\frac{\max_j |\Delta \mathcal{T}_j^{i+1}|}{\max_j |\mathcal{T}_j^{i+1}|} \leq \epsilon_{T,\mathrm{inc}}, \qquad \frac{||R_T(\mathcal{V}^{i+1}, \mathcal{B}^i, \mathcal{T}^i, \mathcal{P}^{i+1})||_f}{||R_T(\mathcal{V}^{i+1}, \mathcal{B}^i, \mathcal{T}^i, \mathcal{P}^{i+1})||_t} \leq \epsilon_{T,\mathrm{res}},$$

where the maximum norm $|.|$ has been taken over all nodal points j. The norms $|| \cdot ||_f$ and $|| \cdot ||_t$ again denote the Euclidean norm over the free and total degrees of freedom. $\epsilon_{T,\mathrm{inc}}$ and $\epsilon_{T,\mathrm{res}}$ are small parameters. In all our calculations we take $\epsilon_{T,\mathrm{inc}} = \epsilon_{T,\mathrm{res}} = \mathcal{O}\left(10^{-3}\right)$.

Outflow boundary conditions.

In principle it is possible to impose the Dirichlet boundary conditions of a fully developed flow at the outflow of a nonisothermal viscoelastic shear flow, as is usually done for isothermal calculations. However, if the Dirichlet boundary conditions at the outflow do not match with the flow, large wiggles may arise near the outflow. For nonisothermal flows with high Péclet numbers, very long exit lengths would be required, before the flow is fully developed. For example solving the temperature equation for a viscous fluid flowing in a tube with radius R and the temperature jumping at the wall of the inflow, the exit length L has to fulfil $L/R \geq 0.68 Pe$ to avoid an oscillatory numerical solution, see Cuvelier *et al.* (1986), p. 56.

Due to the high values of the density and heat capacity and the small thermal conductivity $(\rho c_{p,b}/\kappa = \mathcal{O}(10^7)\ \mathrm{m}^{-2} \cdot \mathrm{s})$ for polymeric fluids, Péclet numbers between $\mathcal{O}(10^3)$ and $\mathcal{O}(10^4)$ are not unusual. To avoid the wiggles also exit lengths between $\mathcal{O}(10^3 R)$ and $\mathcal{O}(10^4 R)$ would be necessary. For a viscoelastic fluid the situation may even become worse due to the decrease of the thermal conductivity in the radial direction due to the anisotropy of the heat conduction tensor. The large exit lengths can (possibly) be avoided with a severe mesh refinement near the outflow boundary. Both possibilities, however, give rise to the use of more unknowns and consequently a (strong) increase of computation times and the requirement of a large memory capacity.

To avoid wiggles due to imposing at the outflow Dirichlet boundary conditions that do not fit to the flow, the standard approach for viscous models is to impose natural boundary conditions that correspond to the fully developed flow instead. Natural boundary conditions are not explicitly satisfied by the solution, but are satisfied in a weak sense, so there is more freedom to adapt to a boundary condition that does not correspond exactly to the flow in the neighbourhood of the boundary. Because there is a strong coupling between the temperature equation and the equations of motion and stress constitutive equation the velocity and stresses are far from fully developed as well. Therefore natural boundary conditions have to be imposed for both the the equations of

motion and the temperature equation. For the equations of motion of viscous fluids a constant normal stress ($\sigma_n = \boldsymbol{n} \cdot \boldsymbol{\sigma} \cdot \boldsymbol{n} = -p_0$, the ambient pressure) and a vanishing tangential velocity are the fully developed flow natural boundary condition. For the temperature equation a vanishing normal heat flux $\phi_{q,n} = \boldsymbol{n} \cdot \boldsymbol{\phi}_q = 0$, which equals $\boldsymbol{n} \cdot \nabla T = 0$, is the fully developed natural boundary condition.

For viscoelastic fluids, however, the fully developed natural boundary conditions are not as straightforward as for viscous fluids. A constant normal stress σ_n along the outflow boundary does not correspond to fully developed flow, because viscoelastic fluids have normal stresses. For these fluids $\sigma_n = -p + \tau_{p,n}$ where $\tau_{p,n} = \boldsymbol{n} \cdot \boldsymbol{\tau}_p \cdot \boldsymbol{n}$ is a function of the shear rate and therefore varies along the outflow boundary. For viscoelastic fluids with a non-zero second normal stress difference the pressure varies along the outflow boundary as well. For high Deborah numbers, the difference between the axis of symmetry (zero normal polymer stress) and the wall (maximum) is large, so that a constant σ_n will lead to large wiggles or convergence problems. Thus we need an approximation of the normal stress profile σ_n along the outflow boundary.

Because the velocity and particularly the stress profiles may strongly depend on temperature, which will at the outflow boundary be far from its fully developed profile, the real fully developed profiles for both quantities do not give a reasonable approximation if the temperature is not fully developed. In order to impose a boundary condition for the equations of motion that fits to the flow, the basic idea is that in an exit section the velocity and stress develop slowly because of the slowly developing temperature (high Péclet numbers). This means that the flow is approximately fully developed at the local temperature distribution in radial direction. For this, we solve for each iteration a 1D fully developed flow problem with the radial temperature distribution the FEM temperature $\mathcal{T}^{i+1}$ at the outflow, i.e. we solve the shear rate $\dot{\gamma}$ from:

$$\tau_{rz} = -\mu r + \frac{d}{r}, \qquad \tau_{lm} = \tau_{lm}(\dot{\gamma}, \mathcal{T}^{i+1}), \qquad l,m = r,z,$$

$$p = -2\mu z + \tau_{rr} - \int_r^R \frac{\tau_{rr}(s)}{s} ds + p_0, \qquad \dot{\gamma} = \frac{dw}{dr}, \qquad (22)$$

where μ and d are constants which have to be determined from the boundary conditions at the end points of the outflow boundary and p_0 is an integration constant, which remains undetermined for incompressible flows. Note that the constitutive equation for the stress has reduced to a nonlinear algebraic equation, which is easy to solve. The obtained σ_n is then used for the boundary integral for the equations of motion. This method only requires the solution of a 1D nonlinear problem along the outflow boundary, so that the related CPU time is negligible compared to the FEM and streamline integration parts. Furthermore it does not influence convergence rate in a negative way and it fits perfectly in the easy treatment of boundary integrals for finite element methods.

For a viscoelastic fluid with anisotropic heat conduction a vanishing normal heat flux $\phi_{q,n} = 0$ does not exactly correspond to the fully developed natural boundary condition. For convenience it will be assumed now that the normal direction corresponds to the z-direction and the tangential direction to the r-direction. For a fully developed flow, $T = T(r)$ and thus $\partial T/\partial z = 0$, the rz-component of the heat conduction tensor then gives a contribution to the heat flux in the normal direction: $\phi_{q,n} = \kappa_{rz} \partial T/\partial r$. For isotropic heat conduction this term vanishes. For anisotropic heat conduction an approximation of this term on the outflow boundary is needed. However, preliminary calculations showed that this is a small term and $\phi_{q,n} = 0$ is sufficient.

If the cooling due to thermal expansion is taken into account there is also a contribution from the boundary integral, resulting from the integration by parts of the pressure term, in the temperature equation. Then the integrand $T\beta p \boldsymbol{n} \cdot \boldsymbol{v}$ has to be evaluated at the outflow boundary. We obtain the pressure in the same way as for the equations of motion, i.e. from equation (22). For the normal velocity and the temperature we take the FEM approximations (at the current iteration step) at the outflow boundary.

Numerical calculations

In this section we will present the results of numerical simulations of a contraction flow for a polyethylene melt (melt I of the IUPAC workshop). With the isothermal code, good correspondence with experimental results for LDPE has been obtained in Hulsen and van der Zanden (1991). Our main goal is to show that the numerical method described in the previous section is able to handle flows with high Deborah and Péclet numbers.

Choice of the test problem

Except the temperature equation itself and a good numerical method to solve it, a number of other things are important for the numerical simulation of nonisothermal viscoelastic flow. We will briefly discuss this below and we will indicate the consequences of it on the choice of our test problem.

- *The temperature boundary conditions.* In general the internal heat production term Q is large in a small boundary layer near the wall. Because near the wall the convection is small, it then depends on the boundary conditions whether the influence on the temperature is large. Imposing a fixed temperature at the wall than minimizes the temperature increase. Therefore a severe cooling will be needed in the experimental setup. Of course, the fixed temperature at the wall also minimizes the influence of the dissipation or stress work on the temperature.

- *The choice of the polymeric fluid.* Polymeric fluids show much difference in their thermal behaviour. The anisotropy may differ considerably for different polymers. Experimental results show a reduction of 40% for the thermal conductivity perpendicular to the deformation for polyethylene, while for Plexiglas PMMA the reduction is only about 2%, see Choy *et al.* (1981). The temperature dependency of the viscosity and relaxation times differs considerably for various polymers. A strong dependence (WLF shift factor) has much more influence on the velocity and stresses than a moderate dependence (Arrhenius shift factor). The value of the thermal expansion coefficient may differ considerably so that the influence of this term also depends on the polymeric fluid used.

- *Lack of experimental data.* Particularly two properties must be mentioned: the anisotropy of the heat conduction and the temperature dependence of the shear modulus given by the exponent γ which determines the internal heat production term Q. For many polymers nothing is known about these properties. If something is known about the anisotropy, only a few data points are given, so that a good fit with a multi-mode model ($\kappa_{1,k}$ different for all modes and eventually dependent on invariants of $\boldsymbol{b}_k$) does not make much sense. Furthermore, a lot of the measurements are below the melting point and the properties are only measured until a limited elongation ratio, say about $\epsilon = 5$. What these properties are exactly for high deformation rates in the fluid state is not completely clear yet. For example: is there any difference between the values of γ and κ_1 for the different modes or are they all the same. It might be well possible that the the anisotropy is more related to the modes with high relaxation times.

- *Influence of the viscoelastic model.* Various viscoelastic models may predict different results. For an anisotropic heat conduction model with constant coefficients for example, a decrease of the thermal conductivity perpendicular to a shear flow can only be predicted for models with a non-zero second normal stress difference. Of course also the dissipation, stress work and the difference between them depend on the viscoelastic model used. A good model for the viscoelastic stress is therefore indispensable in nonisothermal simulations.

- *Influence of the nondimensional numbers.* Obviously, the Deborah number is very important for the difference between the dissipation and the stress work and the anisotropy. For low Deborah numbers the behaviour of the fluid is still dominated by viscous responses ($\boldsymbol{b} \simeq \boldsymbol{I}$)

and nothing significantly happens for these terms. The Péclet number plays an important role on the actual effect on temperature of the various terms in the temperature equation. For very high Péclet numbers there is just not enough time to influence the temperature, even if these terms are large.

- *Influence of the geometry.* In long tubes for example the temperature has more time to develop than in a geometry with a small axial distance. Another example is the presence of inflow and outflow boundaries. Then the temperature is just convected through the outflow boundary. If such boundaries are not present, like in journal bearing, the influence on the temperature solution of the heat production terms (and also the difference between the stress work and dissipation) and the thermal diffusion will be much larger.

Because the stress behaviour is also very important in the temperature equation, we have chosen a polymer that is relatively well characterised, and for which a good eight-mode Giesekus model exists: the LDPE melt I of the IUPAC workshop. Only for γ there is no experimental data available. Therefore we have taken $\gamma = 0$ for which Q equals the mechanical dissipation and $\gamma = 1$ for which Q equals the stress work. For the anisotropy model, we have just taken equal distribution for every mode in the multi mode model. A disadvantage (for a strong influence on stresses) of this fluid is that the temperature dependence of the viscosity and relaxation times is only moderate.

For the geometry, we have chosen for the contraction flow, because Hulsen and van der Zanden (1991) obtained results for the eight-mode Giesekus model that agreed well with experimental data. A consequence of the choice of this geometry is that the Péclet number is large, so that the influence of the various terms can be small, even if the terms themselves are large. Because not much is known about the exact temperature boundary condition and because it may strongly influence the temperature near the wall, we have chosen for a prescribed temperature.

The numerical results will therefore contain as much physical input as possible. However, the influence of some terms in the temperature equation may not be that large for this problem. For other situations, as explained above, these may be important.

Fluid parameters

For our numerical simulations we will use an LDPE melt that can be described by an eight-mode Giesekus model with η_s equal to zero, see Bird *et al.* (1987). In Table 1 we give the data for this model. The temperature dependence of the relaxation times can be described by an Arrhenius shift factor $^{10}\log\left(\frac{\lambda_k}{\lambda_{k,\text{ref}}}\right) = \,^{10}\log a_T = C\left(\frac{1}{T} - \frac{1}{T_{\text{ref}}}\right)$. We have summarised the shift constants and the other parameters that are needed for a nonisothermal flow in Table 2. The zero-shear-rate viscosity at the reference temperature of $T_{\text{ref}} = 423$ K is $\eta_{0,\text{ref}} = 5.105 \cdot 10^4$ Pa·s. The mean relaxation time at the reference temperature is $\lambda_{0,\text{ref}} = \sum_{k=1}^{K} \lambda_{k,\text{ref}} \eta_{k,\text{ref}} / \eta_{0,\text{ref}} = 58.75$ s. We will assume a constant heat capacity $c_{p,b}$, a thermal conductivity independent of temperature, and a constant density, except for the term $T\beta \boldsymbol{v} \cdot \nabla p$ in the temperature equation. Furthermore we have taken $\gamma = 0$. However, due to the dominance of convection in the flows we will discuss, a choice of $\gamma = 1$ would hardly change the results.

Above the melting temperature no detailed measurements of the anisotropy of the heat conduction tensor for LDPE are available in the literature. Measurements of Wallace *et al.* (1985) at $T_{\text{ref}} = 433$ K showed that for an HDPE melt $\kappa_\perp$, the thermal conductivity perpendicular to the flow, decreases asymptotically until about 40 % of the equilibrium thermal conductivity. Measurements of Choy et al. (1978) below the melting temperature T_{m} showed that the perpendicular thermal conductivity of an HDPE melt for a stretching ratio of $\epsilon = 6$, is about $30 - 40$ % of the thermal conductivity in equilibrium. For an LDPE melt the decrease of the $\kappa_\perp$ is of the same order. Because all these data show a considerable decrease of the perpendicular thermal conductivity for polyethylene melts, we have also taken into account a fairly large anisotropy, see Table 3. The minimum perpendicular thermal conductivity is then $\kappa_{\perp,\text{min}} = \kappa_0 = 0.28 \cdot \kappa_{\text{eq}}$, because $b_{k,\perp} \to 0$

Table 1: Viscoelastic properties of LDPE at $T = 423$ K. Successively the mode number, the modal viscosity, the modal relaxation time and the non-dimensional parameter α_k are given. The data are from Bird *et al.* (1987).

k	η_k(Pa·s)	λ_k(s)	α_k
1	$1.00 \cdot 10^3$	10^3	0.03
2	$1.80 \cdot 10^4$	10^2	0.05
3	$1.89 \cdot 10^4$	10^1	0.2
4	$9.80 \cdot 10^3$	10^0	0.5
5	$2.67 \cdot 10^3$	10^{-1}	0.4
6	$5.86 \cdot 10^2$	10^{-2}	0.3
7	$9.48 \cdot 10^1$	10^{-3}	0.2
8	$1.29 \cdot 10^1$	10^{-4}	0.1

Table 2: Thermal properties of LDPE at $T = 423$ K. Successively the density, the linear thermal expansion coefficient, the heat capacity, the thermal conductivity in equilibrium and the shift constant for the Arrhenius shift factor are given. The data have been obtained from Bird *et al.* (1987).

ρ_{ref}	$7.80 \cdot 10^2$	kg·m^{-3}
β	$7.02 \cdot 10^{-4}$	K^{-1}
$c_{p,b}$	$2.54 \cdot 10^3$	J·kg^{-1}·K^{-1}
κ_{eq}	$2.41 \cdot 10^{-1}$	W·m^{-1}·K^{-1}
T_{ref}	$4.23 \cdot 10^2$	K
C	$1.95 \cdot 10^3$	K

Table 3: Heat conduction constants of LDPE in (W·m^{-1}·K^{-1}) for all modes k.

κ_0	$8.92 \cdot 10^{-2}$
$\kappa_{1,k}$	$2.17 \cdot 10^{-2}$

for large $\lambda_k\dot{\gamma}$ and $\lambda_k\dot{\epsilon}$. Because the modes with a small relaxation time almost do not contribute to the anisotropy this value will not be reached. The lowest value in the numerical simulations is about $\kappa_{\perp,\text{min}} = 0.7 \cdot \kappa_{\text{eq}}$, which shows that only the first three modes contribute to the decrease of the perpendicular heat conductivity.

For our flow example we will use two non-dimensional numbers. The first is the Deborah number defined by

$$De = \frac{\lambda_0 V}{L}, \tag{23}$$

where λ_0 is a mean relaxation time at a reference temperature. The second is the Péclet number defined by

$$Pe = \frac{\rho_{\text{ref}}c_{p,b}VL}{\kappa_{\text{eq}}}. \tag{24}$$

Due to the high viscosity of polymeric fluids, the Reynolds number does not play an important role. In the flow geometries we will discuss we have $Re \simeq 10^{-7}$.

Flow through a contraction
The isothermal flow through an axisymmetrical contraction is one of the benchmarks for viscoelastic computations. This flow consists of a fully developed flow at the upstream boundary, a sudden contraction and a fully developed flow at the downstream boundary. We will take the flow through a 4:1 contraction as an example, because it is the most studied contraction flow in the literature.

The geometry of the contraction flow and the temperature boundary conditions that we have used, are depicted in Fig. 2. The inflow length will be taken $20\,R$ and the outflow length $60\,R$, where the radius at the outflow has been taken $R = 5$ mm. This type of flow is dominated by convection. Preliminary calculations showed that for a wall temperature of $T_{\text{w}} = 463$ K, a Deborah number of $De = 50$, a Péclet number of $Pe = 523$, and the anisotropy of the heat conduction taken into account, the maximum temperature rise at $z = 0$ was about 0.15 K. At the outflow boundary the maximum temperature rise was about 0.7 K, however it was still developing and far from its fully developed profile. Of course, these small temperature rises do not have a significant effect on the flow. If the flow rate was increased until $De = 200$, no convergence could be obtained. Probably, this problem is caused by the very high values and the wiggly behaviour of the zz-component of the first mode of the internal deformation tensors near the contraction. If the heat conduction was assumed to be isotropic, or if the anisotropy caused by the first mode was omitted, it was no problem

to obtain a convergent solution method. Because it is unclear whether such very high values of the parallel heat conduction is a model deficiency, we will take the Deborah number $De = 50$ in the nonisothermal calculations, although this is probably not the maximum Deborah number for which convergence can be obtained. In order to demonstrate the ability of our scheme to handle large temperature differences in the flow, we imposed a temperature jump at the wall. The wall near the inflow has been kept at a fixed temperature T_1, the other part of the fixed wall has been kept at a fixed temperature $T_0 \leq T_1$. We will take $\Delta T = 10$ K and $\Delta T = 40$ K in our simulations. All dimensionless numbers, unless explicitly stated, are based on the outflow conditions, i.e. the outflow radius and the temperature T_0 and average velocity at the outflow. For the equations of motion we will assume that the no-slip boundary condition holds on the fixed wall. At the inflow boundary fully developed Dirichlet boundary conditions will be prescribed for the velocity, the stress modes and the temperature. At the outflow boundary a vanishing tangential velocity and the fully developed Neumann boundary conditions for the normal stress and the temperature will be imposed. See the section about the outflow boundary condition for the details. As mentioned earlier it has been found that such a type of boundary conditions are necessary to avoid wiggles or extreme exit lengths.

The calculations have been performed on a mesh with 5587 grid points. The part of the mesh near the contraction has been depicted in Fig. 3. Near the sharp corner, where the gradients are large, the mesh is relatively fine. Towards the outflow and inflow boundary we have taken a much coarser mesh, because the gradients are much smaller there. For the problem with anisotropy, $De = 50$, and a temperature jump of $\Delta T = 10$ K and $\Delta T = 40$ K we needed 123 and 136 iterations. Without the anisotropy, we needed 62 and 56 iterations, respectively.
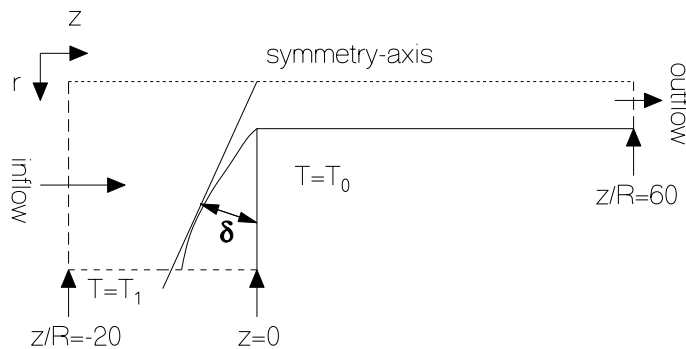
Figure 2: Flow geometry, definition of the opening angle δ and temperature boundary conditions for the 4:1 contraction. The fixed wall near the inflow (dashed line) has been kept at temperature T_1. The other part of the wall (solid line) has been cooled to T_0.
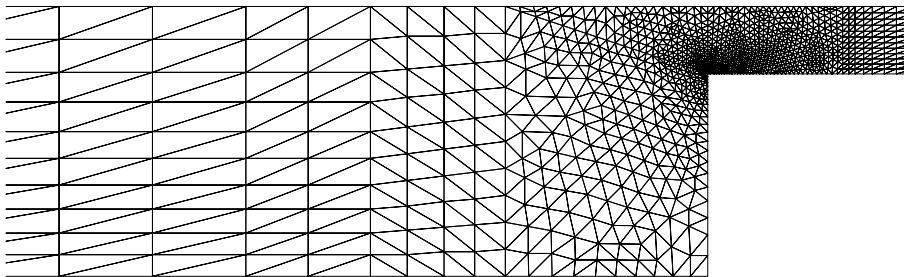
Figure 3: A part of the finite element mesh, $-10 \leq z/R \leq 3$, near the sharp corner of the 4:1 contraction.

A characteristic phenomenon of contraction flows of viscoelastic fluids is that a vortex may exist in the entry corner. Two features of this vortex will be examined. Firstly, the opening angle δ of the vortex, defined in Fig. 2. Secondly, the vortex intensity I_ψ which equals the ratio of the

14

amount of fluid flowing in the vortex and in the main flow, and is defined by

$$I_\psi = \frac{\psi_{\text{sep}} - \psi_{\text{cen}}}{\psi_{\text{ax}} - \psi_{\text{sep}}}, \tag{25}$$

where ψ_{sep} is the value of the stream function at the separating streamline, ψ_{cen} the value at the centre of the vortex and ψ_{ax} the value at the axis of symmetry.

To get a good understanding of the nonisothermal effects we will shortly examine the influence of the viscoelasticity (isothermal), before we will present the results of the nonisothermal calculations.

Isothermal flow
The isothermal flow through a 4:1 and a 5.75:1 contraction for the eight-mode Giesekus model of Table 1, has already been calculated in Hulsen and van der Zanden (1991). They have shown that the size of the computed vortex in the edge before the contraction agrees well with experimental results. The size of the vortex strongly depends on the flow.

Hulsen and van der Zanden (1991) argue that the growth of the vortex is a mechanism to fulfil the balance of linear momentum in the axial direction:

$$\frac{1}{r}\frac{\partial r\tau_{rz}}{\partial r} + \frac{\partial \tau_{zz}}{\partial z} \simeq 0, \tag{26}$$

where the (small) term with the pressure gradient has been neglected. With a larger vortex the build-up of the dominant term in this equation, τ_{zz}, before the contraction can be more gradually. Equation (26) indicates that the ratio of the elongational stress and the shear stress is important for the size of the vortex. The isothermal flow through the 4:1 contraction has been calculated for the four Deborah numbers of Table 4. For the computations the iteration viscosity has been taken

Table 4: Vortex intensity I_ψ and opening angle δ for various Deborah numbers (isothermal).

De	$I_\psi(\%)$	$\delta(\deg)$
3	2.9	28
15	10.0	43
50	10.9	52
200	11.1	53

$\eta_{\text{it}} = 2\eta_0$ and the extra viscosity $\eta_{\text{co}} = \eta_0$.

Notice that for relatively small Deborah numbers the opening angle δ is already considerable: $\delta = 28\,\text{deg}$ for $De = 3$. For increasing Deborah number the opening angle keeps increasing till $\delta = 53\,\text{deg}$ for the highest Deborah number of $De = 200$. However, for the two highest Deborah numbers the differences are relatively small. The corresponding opening angles δ and the vortex intensities I_ψ for the various Deborah numbers have been given in Table 4. Similarly, the increase of the vortex intensity is large for the low Deborah numbers. For the two highest Deborah numbers there is hardly any difference. The strong increase for the low Deborah numbers can be explained by examining the stresses at the contraction.

The normal stress τ_{zz} and the shear stress τ_{rz} at $z = 0$, have been depicted in Fig. 4. The stresses are relative to the wall shear stress τ_{w} at the outflow for a Deborah number of $De = 200$. Particularly between $De = 3$ and $De = 50$ the increase of τ_{zz} is relatively large. Only for the lowest Deborah numbers the normal stress is almost constant over the whole region. For $De = 15$ a small local maximum arises near $r/R \simeq 0.7$. The local maximum is more clear for the two highest Deborah numbers, where the maximum normal stress is about two times as large as the normal stress at the centreline and at the wall. Also the magnitude of the shear stress decreases more for the low Deborah numbers, although less than τ_{zz}. For all Deborah numbers τ_{rz} remains
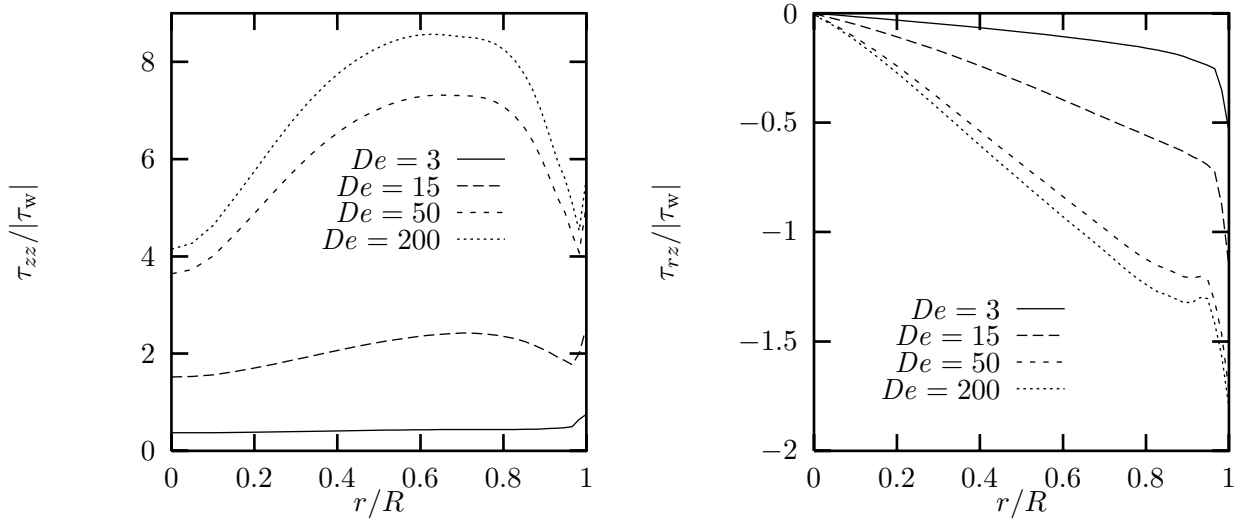
Figure 4: Normal stress $\tau_{zz}/|\tau_{\mathrm{w}}|$ and shear stress $\tau_{rz}/|\tau_{\mathrm{w}}|$ at $z = 0$ for various Deborah numbers. The stresses are relative to the wall shear stress for $De = 200$ at the outflow.

approximately linear in the core region. Only near the wall there is a sharp decrease preceded by a small increase for the two highest Deborah numbers.

Nonisothermal flow

For the computations we used $\eta_{\mathrm{it}} = 2\eta_0$ for the iteration viscosity and $\eta_{\mathrm{co}} = \eta_0$ for the extra viscosity, both at the temperature of the wall at the outflow. For the iteration diffusivity we used $\kappa_{\mathrm{it}} = \kappa_{\mathrm{eq}}$. In this section we will focus on the anisotropy of the heat conduction tensor. First, however, we will briefly discuss the difference between the dissipation and the stress work in the flow. Although we already noted that the influence of the internal heat production terms on the temperature is small for our test problem, we will briefly discuss the difference between the dissipation and the stress work first.

Fig. 5 shows the difference between the dissipation and the stress work for a flow of $De = 50$
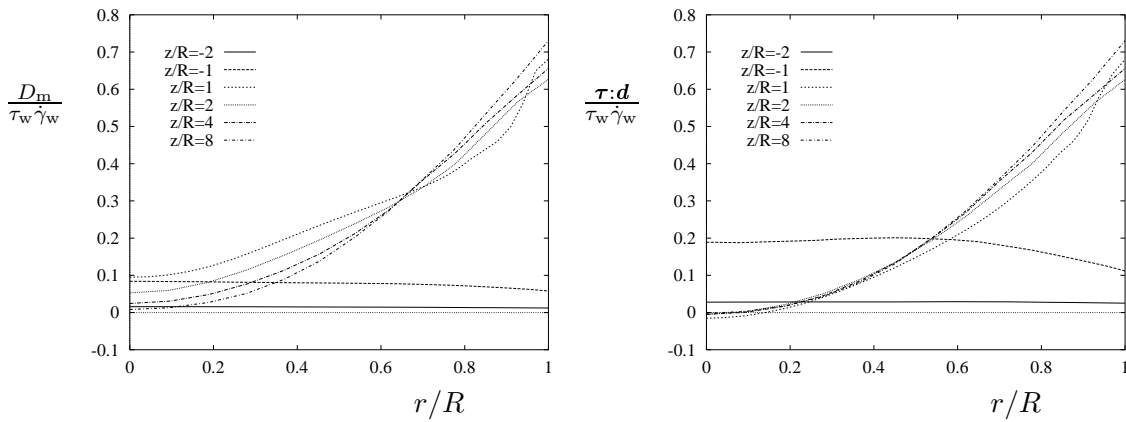
Figure 5: Mechanical dissipation and stress work at various distances from the contraction. The mechanical dissipation and the stress work have been scaled with the wall shear stress τ_{w} and the wall shear rate $\dot{\gamma}_{\mathrm{w}}$ at the outflow.

on lines of constant z near the contraction. Before the contraction the stress work is considerably higher than the mechanical dissipation, particularly for $z/R = -1$ where it is about two times as large. This means that a part of the mechanical energy production is stored. After the contraction the mechanical dissipation decreases relatively slowly, because then the stored energy is released.

Contrary to the mechanical dissipation, which has to remain positive, the stress work near the centreline becomes negative. This is caused by the decrease of v_z in the z-direction while the dominant stress τ_{zz} is still positive. However, because of the dominance of the convection for this problem, using either the mechanical dissipation ($\gamma = 0$) or the stress work ($\gamma = 1$) as heat production term Q, does not result in considerable differences in the temperature. However, Fig. 5 also shows that the difference between the mechanical dissipation and the stress work is not small. For flows with lower Péclet numbers or heat flux boundary conditions for the temperature equation the difference is much more important.

In order to demonstrate that the code is able to handle large temperature differences in the flow, we will impose a temperature jump at the wall. For the temperature jumps we will take $\Delta T = 10$ K and $\Delta T = 40$ K. To examine the influence of the anisotropy, we will distinguish 4 cases: $\Delta T = 10$ K with isotropic heat conduction (case I), $\Delta T = 10$ K with anisotropic heat conduction (case II), $\Delta T = 40$ K with isotropic heat conduction (case III) and $\Delta T = 40$ K with anisotropic heat conduction (case IV). The isothermal flow at $De = 50$ will be denoted by case 0. The Péclet number for all calculations is $Pe = 93$.

For the four cases the resulting temperature distributions near the contraction have been depicted in Fig. 6. The results can be explained by considering the corresponding anisotropy of the
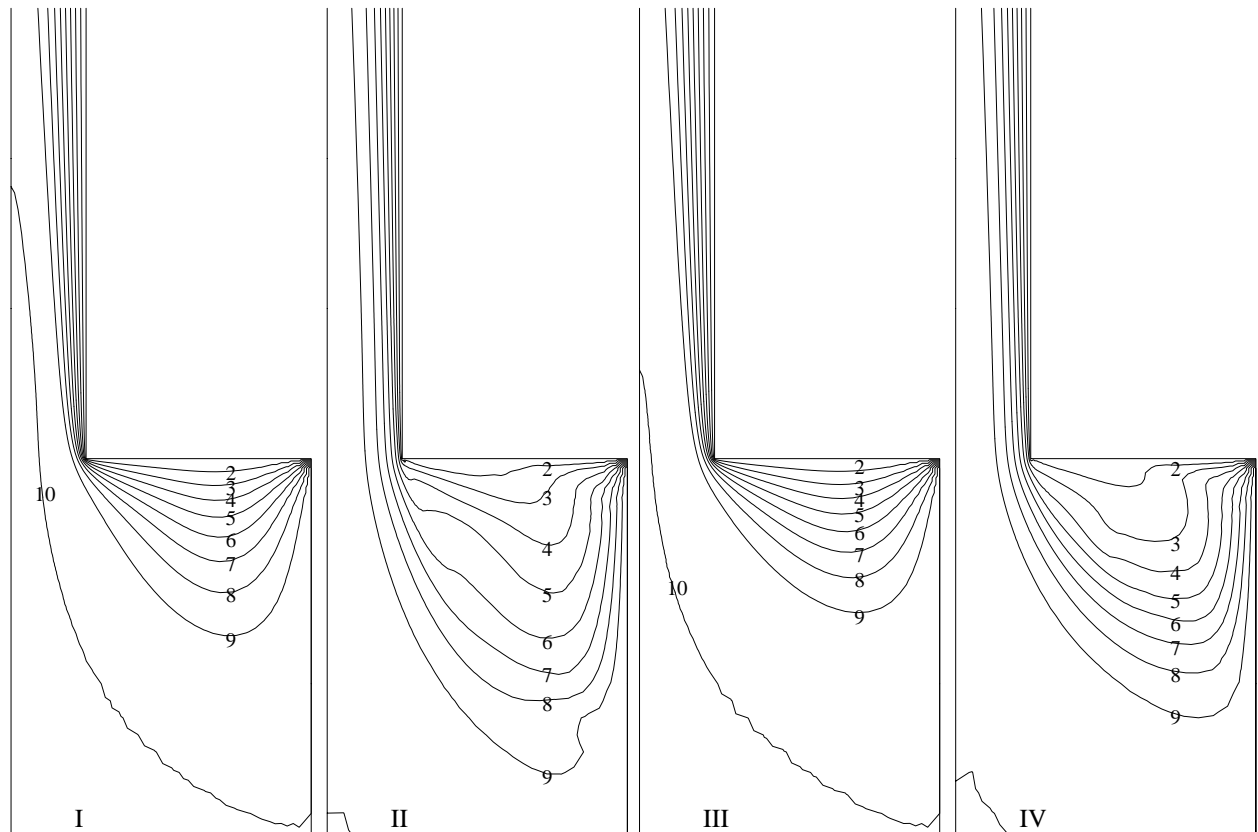
Figure 6: Temperature isolines near the contraction, $-5 \leq z/R \leq 6$, for various temperature jumps without and with the anisotropy of the heat conduction tensor. Case I: $\Delta T = 10$ K without anisotropy, II: $\Delta T = 10$ K with anisotropy, III: $\Delta T = 40$ K without anisotropy, IV: $\Delta T = 40$ K with anisotropy. The ten isotherms are evenly spaced between the maximum temperature, 403 K or 433 K, and the minimum temperature 393 K.

heat conduction tensor. The rr-, rz- and zz-components of $\boldsymbol{\kappa}$ for $\Delta T = 10$ K have been depicted in Fig. 7. In the entry corner the conduction of heat upstream is much larger when the anisotropy has been taken into account. This is caused by the large values of κ_{zz} in the entry corner as can be seen from the small figure in Fig. 7. Along the wall of the outflow a temperature boundary

17
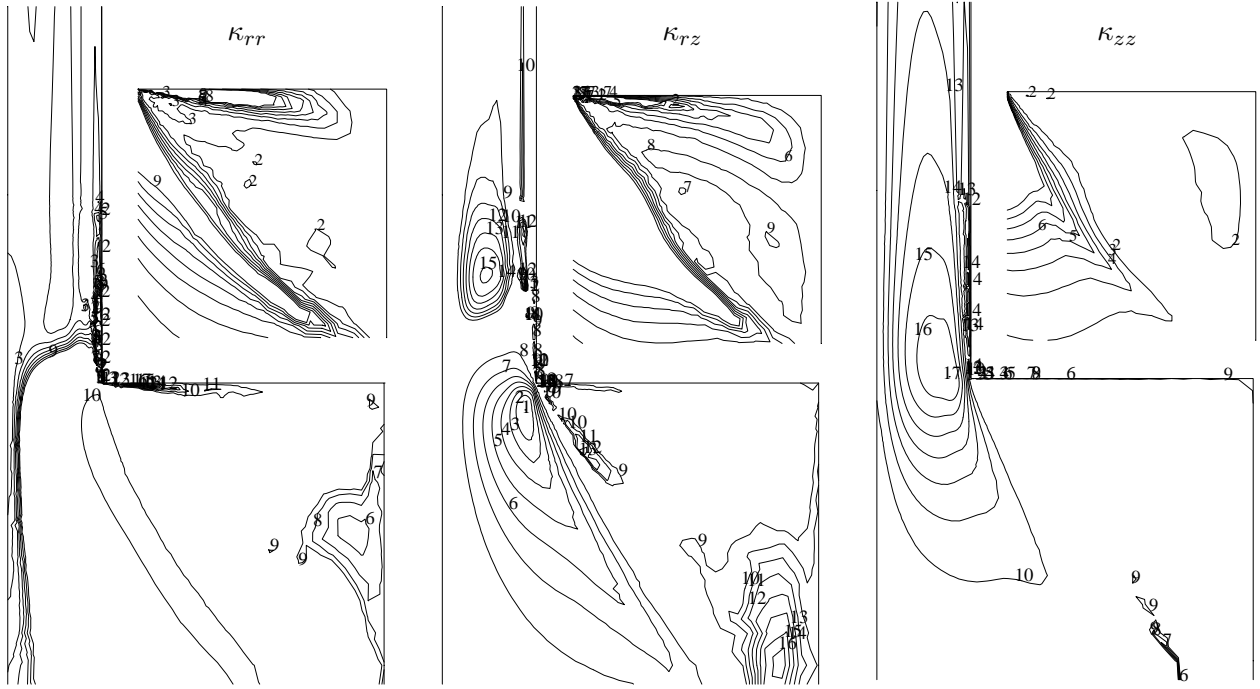
Figure 7: Isolines near the contraction, $-5 \leq z/R \leq 6$, for κ_{rr}, κ_{rz} and κ_{zz}. The temperature jump equals $\Delta T = 10$ K (case II of Table 5). The lines are evenly spaced below and above the isotropic value of the concerned quantity. The isotropic value corresponds to line 8 for κ_{rz} and κ_{zz} and to line 10 for κ_{rz}. The minimum (line 1) and maximum (line 17) values are: $0.68 \leq \kappa_{rr}/\kappa_{eq} \leq 204$, $-143 \leq \kappa_{rz}/\kappa_{eq} \leq 3.2$, $0.74 \leq \kappa_{zz}/\kappa_{eq} \leq 791$. For the figures of the entry corner, $-3 \leq z/R \leq 0$ and $1 \leq r/R \leq 4$, the minimum (line 1) and maximum (line 9) values are evenly spaced between: $0.68 \leq \kappa_{rr}/\kappa_{eq} \leq 24$, $-16 \leq \kappa_{rz}/\kappa_{eq} \leq 3.2$, $0.74 \leq \kappa_{zz}/\kappa_{eq} \leq 89$.

layer develops. At $z = 0$ the boundary layer for the anisotropic cases is about two times as large as for the isotropic cases. Because the cold front develops farther outside the vortex, the convective transport of heat in the core flow provides a larger temperature boundary layer at $z = 0$. Due to the reduced thermal conductivity in the direction perpendicular to the flow in the outflow section (where the polymer chains are oriented in the direction of the flow), the boundary layer develops much slower for the anisotropic cases (the minimum is just below $0.7\kappa_{eq}$, indicating that only the first three to four modes are active). At $z/R \simeq 6$ (the top side of the pictures in Fig. 6) the sizes of the boundary layers are almost equal. The magnitude of the rz-component of the heat conduction tensor is large (and negative) near the separation line of the vortex, indicating that the polymer chains are oriented in the direction of the flow.

The results for the heat conduction tensor for the temperature difference $\Delta T = 40$ K showed the same type of behaviour. The main difference was that for the latter the thermal conductivity in the zz-direction is much lower. This is due to the lower temperature in the core flow, which causes a lower relaxation time and therefore less orientation of the polymer chains. The thermal conductivities in the rr-direction are of comparable magnitude.

Due to the higher temperature near the centreline (still approximately equal to the temperature of the inlet), the magnitude of the stresses is smaller compared to the isothermal flow for $De = 50$. The influence on the normal stress τ_{zz} and the shear stress τ_{rz} at $z = 0$ has been depicted in Fig. 8. The stresses are relative to the wall shear stress τ_w at the outflow for the isothermal flow of $De = 200$. For comparison the stresses for the isothermal flows with $De = 15$ and $De = 50$ have also been given. The latter corresponds to the Deborah number with λ_0 evaluated at the temperature of the outflow boundary. The first almost corresponds to the Deborah number with λ_0 evaluated at the temperature of the inflow boundary for $\Delta T = 40$ K, $De(T_1) = De(463 \text{ K}) = 17$. Particularly, the resulting normal stresses τ_{zz} at $z = 0$ are considerably smaller than for the isothermal case
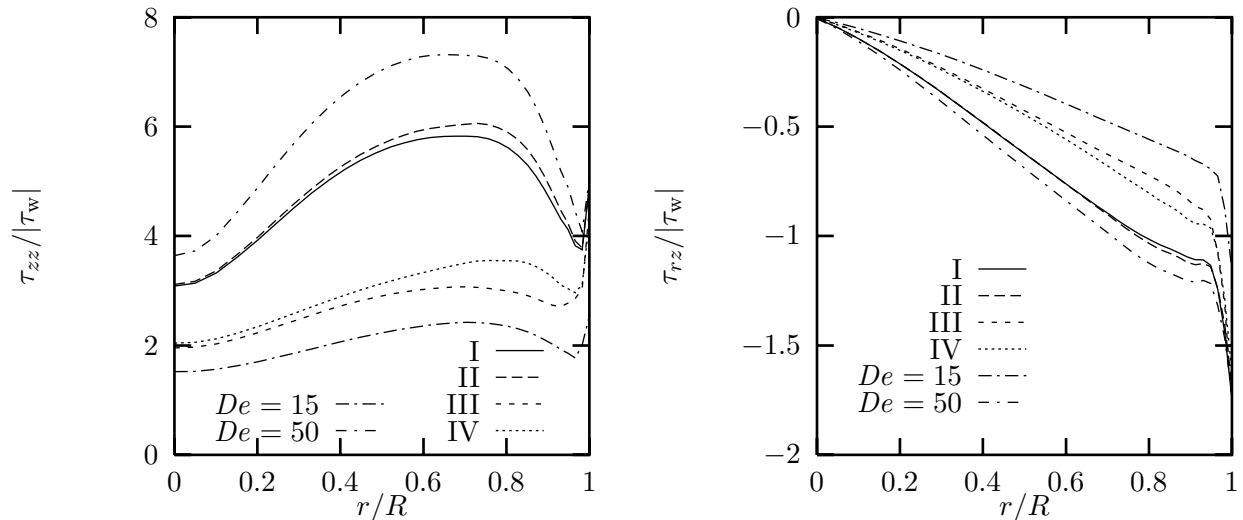
Figure 8: Normal stress $\tau_{zz}/|\tau_\mathrm{w}|$ and shear stress $\tau_{rz}/|\tau_\mathrm{w}|$ at $z = 0$ for various temperature jumps ΔT with and without the anisotropy of the heat conduction tensor (see Table 5). The isothermal stresses for $De = 15$ and $De = 50$ have been depicted for comparison. The stresses are relative to the isothermal wall shear stress τ_w at the outflow.

at $De = 50$ and larger than the isothermal case at $De(T_1)$. Only at the wall all stresses for the nonisothermal calculations are almost equal to the stresses for the isothermal calculations at $De = 50$. The shear stress shows the same type of behaviour, except that the differences are somewhat smaller.

Compared to the influence of the temperature jump, the anisotropy only has a small influence on the stresses at the contraction, although Fig. 6 shows that the temperature at $z = 0$ is considerably lower when the anisotropy of the heat conduction tensor has been taken into account. With increasing magnitude of the temperature jump the differences increase, but only for $\Delta T = 40$ K the magnitude of the stresses near $r/R = 0.8$ are significantly larger when the anisotropy has been taken into account.

In view of the isothermal results for the stresses in Fig. 4, one would expect that the decrease of the stresses in the nonisothermal flow also decreases the opening angle. This is indeed the case. The resulting opening angles δ and the vortex intensities I_ψ have been given in Table 5. The opening

Table 5: Vortex intensity I_ψ, opening angle δ and the Deborah number at the temperature at the inflow boundary. For the various temperature jumps at the wall, the influence of the anisotropy of the heat conduction tensor has been given. The Deborah number based on the outflow equals $De = 50$.

	ΔT (K)		$I_\psi(\%)$	δ(deg)	$De(T_1)$
	0	isotherm	10.9	52	50
I	10	isotropic	10.4	50	38
II	10	anisotropic	10.9	50	38
III	40	isotropic	6.8	42	17
IV	40	anisotropic	7.9	43	17
	0	isotherm	10.0	43	15

angle does not differ much from the isothermal calculations, with the Deborah number evaluated at the temperature of the wall at the inflow. The vortex intensities, however, may become considerably smaller. For the isothermal calculations at $De = 15$ the vortex intensity was $I_\psi = 10\,\%$ and for the nonisothermal calculations with $\Delta T = 40$ K it was about 7-8 %. The local decrease of the temperature in the entry corner, increases the viscosity of the fluid there. If the force of the core

19

flow on the vortex increases less, the temperature is close to $T = T_1$ in almost the complete core flow, this results in a decrease of the vortex intensity. Figure 6 shows that for the anisotropic cases the temperature in the main flow is decreased much more, which results in a higher viscosity in the main flow and thus a larger vortex intensity.

Conclusions

In this paper we have addressed the main problems of the simulation of nonisothermal flow of viscoelastic fluids at high De and Pe numbers.

To handle the outflow boundary condition, a boundary condition that fits to the flow has to be found. Therefore, an equivalent for the Neumann boundary conditions for viscous fluids is developed, where the approximation of the normal stress at the outflow is obtained with the help of the fully developed flow equations. Another important aspect is the numerical calculation of the dissipation. Even if this term is not large, it may have disastrous effects in the numerical scheme when positive definiteness of the configuration tensor is lost. Then a term with the inverse of $\boldsymbol{b}$ may inflate the dissipative term. For a number of models this can be avoided by correcting the configuration tensor to a positive definite tensor.

The example problem of a contraction flow for an LDPE melt shows the capability of the numerical method at high Deborah and Péclet numbers. We found that the difference between the mechanical dissipation and stress work can be large. Due to the high Péclet number and the choice of Dirichlet boundary conditions, however, the influence on the temperature of the internal heat production terms was small for our example problem. For flows where the internal heat production is important the difference between the stress work and dissipation will be important.

Compared to the isotropic case, the anisotropic heat conduction gave a considerable increase in the heat conduction upstream in the vortex This resulted in a larger boundary layer at the contraction. However, due to the decrease of the thermal conductivity perpendicular to the flow for the anisotropic case, the boundary layer then develops much slower in the outlet section.

Furthermore, we found that the parallel component of the heat conduction tensor may become very large. Whether this is a model deficiency or a real effect needs further experimental research at high deformation rates.

References

BIRD, R.B., ARMSTRONG, R.C., & HASSAGER, O. 1987. *Dynamics of Polymeric Liquids*. 2nd edn. Vol. 1. New York: John Wiley.

BRAUN, H. 1991. A model for the thermorheological behavior of viscoelastic fluids. *Rheol. Acta*, **30**, 523–529.

BROOKS, A., & HUGHES, T.J.R. 1982. Streamline upwind Petrov–Galerkin formulations for convection dominated flows with particular emphasis on the incompressible Navier–Stokes equations. *Comp. Meth. Appl. Mech. Eng.*, **32**, 199–259.

CHOY, C.L., LUK, W.H., & CHEN, F.C. 1978. Thermal conductivity of highly oriented polyethylene. *Polymer*, **19**, 155–162.

CHOY, C.L., ONG, E.L., & CHEN, F.C. 1981. Thermal diffusivity and conductivity of crystalline polymers. *J. Appl. Polym. Sci.*, **25**, 2325–2335.

CUVELIER, C., SEGAL, A., & VAN STEENHOVEN, A.A. 1986. *Finite element methods and Navier–Stokes equations*. Dordrecht: D. Reidel Publishing Co.

FERRY, J.D. 1981. *Viscoelastic properties of polymers*. 2nd edn. New York: John Wiley.

HUGHES, T.J.R., & BROOKS, A. 1982. A theoretical framework for Petrov–Galerkin methods with discontinuous weighting functions: application to the streamline-upwind procedure. *Pages 47–*

65 of: GALLAGHER, R.H., NORRIE, D.H., ODEN, J.T., & ZIENKIEWICZ, O.C. (eds), *Finite elements in fluids*, vol. 4. New York: John Wiley.

HULSEN, M.A. 1988. Some properties and analytical expressions for plane flow of Leonov and Giesekus models. *J. Non-Newtonian Fluid Mech.*, **30**, 85–92.

HULSEN, M.A., & VAN DER ZANDEN, J.P.P.M. 1991. Numerical simulation of contraction flows using a multi-mode Giesekus model. *J. Non-Newtonian Fluid Mech.*, **38**, 183–221.

TRELOAR, L. 1975. *Physics of rubber elasticity.* Oxford: Oxford University Press.

VAN DEN BRULE, B.H.A.A. 1995. Micro-rheological modelling of heat conduction in polymeric liquids. *Pages 11–20 of:* DIJKSMAN, J.F, & KUIKEN, G.D.C. (eds), *Numerical simulation of non-isothermal flow of viscoelastic liquids.* Dordrecht: Kluwer Academic Publishers.

VAN KREVELEN, D.W., & HOFTYZER, P.J. 1976. *Properties of polymers.* Amsterdam: Elsevier.

WALLACE, D.J., MORELAND, C., & PICOT, J.J.C. 1985. Shear dependence of thermal conductivity in polyethylene melts. *Polym. Eng. Sci.*, **25**, 70–74.

WAPPEROM, P. 1996. *Nonisothermal flows of viscoelastic fluids: thermodynamics, analysis and numerical simulation.* Ph.D. thesis, Delft University of Technology.

WAPPEROM, P., & HULSEN, M.A. 1995. A lower bound for the invariants of the configuration tensor for some well-known differential models. *J. Non-Newtonian Fluid Mech.*, **60**, 349–355.

WAPPEROM, P., & HULSEN, M.A. 1997. Thermodynamics of viscoelastic fluids: the temperature equation. Submitted to J. Rheology.